

## Quantum oscillations in ultra pure PtSn<sub>4</sub>

M. Inamdar<sup>1\*</sup>, M. Kriegisch<sup>1</sup>, L. Shafeek<sup>1</sup>, A. Sidorenko<sup>1</sup>, H. Müller<sup>1</sup>,  
A. Prokofiev<sup>1</sup>, P. Blaha<sup>2</sup> and S. Paschen<sup>1</sup>

<sup>1</sup>Institute of Solid State Physics  
Vienna University of Technology, Wiedner Hauptstr. 8-10, 1040 Vienna, Austria.

<sup>2</sup>Institute of Materials Chemistry  
Vienna University of Technology, Getreidemarkt 9/165-TC, 1060 Vienna, Austria.

\*inamdar@ifp.tuwien.ac.at

**Keywords:** de Haas-van Alphen oscillations, Fermi surface, magnetostriction, flux growth, PtSn<sub>4</sub>

**Abstract.** PtSn<sub>4</sub> is a non-congruently melting compound in the Pt-Sn binary phase diagram, crystallizing in the centrosymmetric space group *Ccca*. We report on single crystal growth, temperature dependent electrical resistivity  $\rho(T)$ , isothermal field-dependent magnetization  $M(H)$  and magnetostriction  $\lambda(H)$ , and on band structure calculations of this transition metal compound. The high quality of the sample makes it possible to observe clearly resolved quantum oscillations in the magnetization data for temperatures as high as 20 K and in magnetic fields as low as 10 kOe. We found several frequencies along the three crystallographic directions and could relate them to several extremal orbits on the Fermi surface.

PtSn<sub>4</sub> crystallizes in an orthorhombic structure of space group *Ccca* with  $Z=4$ . This structure is a stacking variant of the structures of CoSn<sub>2</sub> (CuAl<sub>2</sub> type) and PtSn<sub>2</sub> (CaF<sub>2</sub> type) [1]. It consists of atomic layers containing either Pt or Sn stacked along the *b* axis. As PtSn<sub>4</sub> falls on the Sn rich side of the Pt-Sn binary phase diagram, single crystals were obtained from a Sn rich Pt-Sn solution. The melt was slowly cooled from 600 °C to 350 °C to allow crystallization of PtSn<sub>4</sub>. Excess Sn was centrifuged there after. Thin platelet-like crystals of PtSn<sub>4</sub> were obtained. The Pt:Sn atomic ratio of 1:4 was confirmed by EDAX measurements. The single crystals were aligned by Laue back reflection patterns. Few tiny crystals were crushed to perform powder x-ray diffraction, giving the cell parameters  $a = 6.418 \text{ \AA}$ ,  $b = 11.366 \text{ \AA}$  and  $c = 6.366 \text{ \AA}$ . The relative high ductility and low crystallization temperature of this compound are credited to the high Sn content.

The electrical resistivity of a single crystalline PtSn<sub>4</sub> sample was measured by a standard four point technique in a physical property measurement system (PPMS) from Quantum Design. As the flux grown crystals grow thinnest along the longest axis (*b*),  $\rho_b(T)$  is difficult to measure and is reported here for the first time. The single crystal used had dimensions,  $a \times b \times c = 2.5 \times 0.6 \times 3 \text{ mm}^3$ .  $\rho_b(T)$  was measured with voltage leads along the *b* (0.6 mm thickness) direction and with current leads placed near to the voltage leads but on the *ac* plane. Figure 1 summarizes results from the electrical resistivity measurements. The resistivity decreases almost linearly with temperature from 300 K to 20 K for all the axes, indicating metallic behaviour. The curves tend to saturate below 20 K, as also observed by E. Mun et al. [2]. The room temperature resistivity values for the three axes are  $\rho_a = 256 \mu\Omega\text{cm}$ ,  $\rho_b = 3813 \mu\Omega\text{cm}$  and  $\rho_c = 344 \mu\Omega\text{cm}$ , i.e. for the *b* axis the room temperature resistivity is more than one order of magnitude larger than the other two axes. The residual resistance ratio (RRR) taken as  $\rho_{300K}/\rho_{2K}$  is 812 for the *a* axis, 41 for the *b* axis and 1330 for the *c* axis, reflecting high quality sample.

Isothermal field-dependent magnetization for field along the three axes was measured in the vibrating sample magnetometer (VSM) option of a PPMS. The magnetization data along one of the axes (*b*) is shown as an example in Fig. 2. PtSn<sub>4</sub> is diamagnetic down to 2 K. We could clearly resolve de Haas-van Alphen (dHvA) oscillations at fields as low as 10 kOe and at temperatures as high as 20 K. As expected, the frequency of the oscillations is temperature independent but amplitude decreases

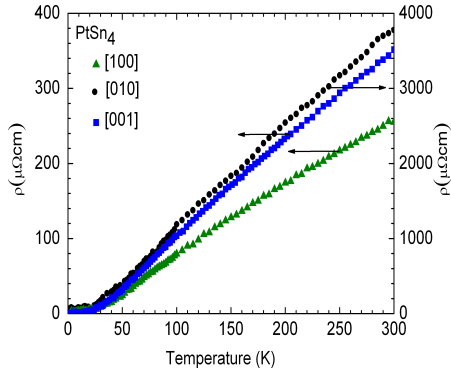


Fig. 1: Electrical resistivity data of PtSn<sub>4</sub>. The more than one order of magnitude difference between  $\rho_b(T)$  and  $\rho_{a,c}(T)$  is because of the large value of the lattice cell parameter  $b$ .

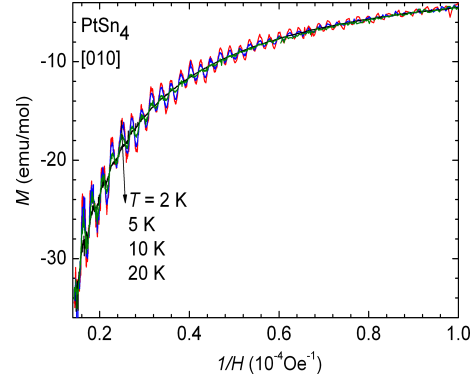


Fig. 2: Magnetization as function of inverse magnetic field  $M(1/H)$ , with field along the  $b$  axis of PtSn<sub>4</sub> sample. The plot shows measurements at different temperatures.

with increasing temperature. The dHvA frequencies obtained their are quite different for the three directions indicating that the Fermi surface is anisotropic. Most of the dHvA frequencies for magnetic field along the  $b$  axis reported in [2] are retrieved in our measurements.

We also observe dHvA oscillations in the magnetostriction data. Magnetostriction measurements were performed in a capacitance cell mounted in a <sup>4</sup>He cryostat with a superconducting 90 kOe coil [3] and are reported for the first time. Figure 3 shows the magnetostriction as function of field for the three principal directions.

Various frequencies observed in the magnetization  $M(1/H)$  and the magnetostriction  $\lambda(1/H)$  data were resolved from the fast Fourier transform plot along the three axes. One such plot along the  $a$  axis is shown in Fig. 4. Most of the main features of  $M(1/H)$  can also be identified in  $\lambda(1/H)$ . The Fermi surface of PtSn<sub>4</sub> was derived from our ab-initio density functional theory calculations (Wien2K). The bands contributing to the Fermi surface are shown in Fig. 5. We identify the minimum energy band crossing the Fermi surface as Band 1 and the maximum energy band crossing the Fermi surface as Band 4. In this way our Band nomenclature does not match that of E. Mun et.al. [2] but is correct to the best of our knowledge. As seen in the figure the Fermi surface of PtSn<sub>4</sub> is complicated, with multiple sheets. Taking spin-orbit coupling into account does not change the Fermi surface appreciably. States near the Fermi energy are predominantly of Sn character. The Brillouin zone has dimensions  $a' = 3.334 \times 10^7 \text{ cm}^{-1}$ ,  $b' = 3.174 \times 10^7 \text{ cm}^{-1}$  and  $c' = 9.837 \times 10^7 \text{ cm}^{-1}$ . We derived extremal cross-sectional areas  $S_e$  perpendicular to the applied magnetic field of the various sheets of Fermi surface from the band structure calculations and used them to calculate the dHvA frequencies  $f$  from

$$P = 1/f = \Delta(1/H) = 2\pi e/\hbar c S_e, \quad (1)$$

where  $P$  is the period ( $\text{Oe}^{-1}$ ) of the dHvA oscillation in  $1/H$ . In Table 1 these frequencies are compared to the values determined from our  $M(1/H)$  and  $\lambda(1/H)$  data. It can be seen that here, in addition to the findings of a parallel investigation [2] we have succeeded in assigning many of the experimentally observed frequencies (Fig. 4) to a particular sheet of the Fermi surface (Fig. 5). Overall, band 1 contributes to the smallest frequencies ( $f < 0.5 \text{ MOe}$ ), Fermi sheets  $\beta_1, \beta_2, \delta, \eta_2, \epsilon$  and band 4 to the intermediate frequencies ( $0.5 \text{ MOe} < f < 3 \text{ MOe}$ ) and Fermi sheets  $\alpha, \gamma$  and  $\eta_1$  to the largest frequencies ( $f > 3 \text{ MOe}$ ). The Fermi sheet  $\alpha$  is the most anisotropic, with a very large cross sectional area perpendicular to the  $a$  axis, giving dHvA frequency of 5 MOe and a much smaller cross sectional area perpendicular to the  $b$  axis giving a dHvA frequency of only 1.8 MOe. The cross-sectional area of the Fermi sheet  $\eta_1$  is too large to be accessed in our experiments.

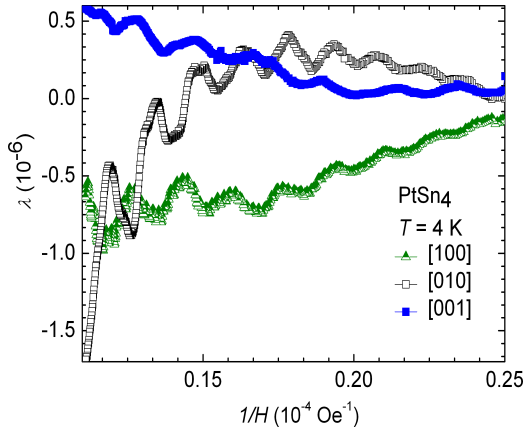


Fig. 3: The graph shows change in linear unit cell parameter ( $\lambda = \Delta/l$ ) of  $\text{PtSn}_4$  with changing magnetic field along the three crystallographic directions. The small amplitude of  $\lambda(1/H)$  is attributed to the diamagnetic nature of the sample.

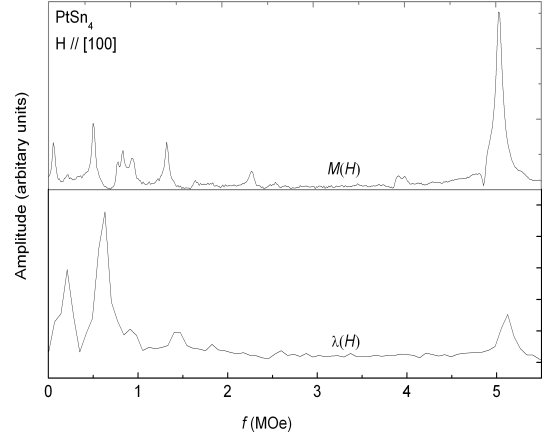


Fig. 4: The top panel shows a fast Fourier transform (FFT) of the magnetization  $M(1/H)$  data of  $\text{PtSn}_4$  along the  $a$  axis. We could resolve multiple frequencies. The lower panel shows similar information but from the magnetostriction  $\lambda(1/H)$  data.

### Summary

High quality single crystalline samples of  $\text{PtSn}_4$  were grown from Sn flux. From magnetization measurements we established that  $\text{PtSn}_4$  is diamagnetic down to 2 K. The high quality of the samples makes it possible to observe various dHvA frequencies in both the magnetization  $M(H)$  and the magnetostriction  $\lambda(H)$  with fields along the three principal crystallographic directions. We could assign of most of the experimentally observed dHvA frequencies with different sheets of the Fermi surface of  $\text{PtSn}_4$ , due to their proximity with the theoretical value.

Table 1: Compilation of dHvA frequencies (in MOe) of  $\text{PtSn}_4$  with fields along the three crystallographic directions determined from the  $M(1/H)$  and the  $\lambda(1/H)$  data, and of the theoretically calculated values. The experimental values are assigned to specific bands due to the proximity with the theoretical value.

Axis	Value	B1	B2					B3			B4
			$\alpha$	$\beta_1$	$\beta_2$	$\gamma$	$\delta$	$\eta_1$	$\eta_2$	$\epsilon$	
[100]	Exp.	0.15	5	2.3	4		1			0.59	1.4
	Cal.	0.11	5	2.1	$2\beta_2 = 4$	5.3	1.2	8.3	1.7	0.56	1.45
[010]	Exp.		1.82	0.57	1.98		1.15		3.6	0.55	1
	Cal.		1.65	0.74	$2\beta_2 = 2.1$	9.6	1.18	10.9	3.3	0.69	0.96
[001]	Exp.	0.14	3.2	0.64	1.6	1.37				0.45	
	Cal.	0.14	3.4	0.67	$2\beta_2 = 1.9$	$2\gamma = 1.34$	0.07	6.8	0.7	0.48	

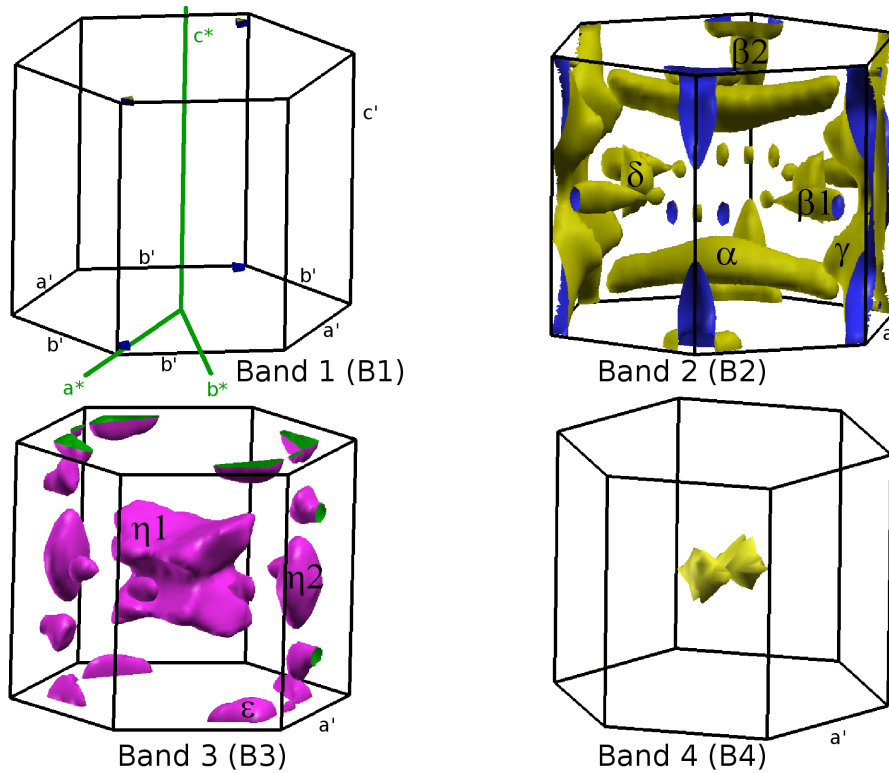


Fig. 5: Fermi surface of  $\text{PtSn}_4$  derived from density functional theory calculations.  $a^*$ ,  $b^*$ ,  $c^*$  are the reciprocal lattice vectors of the orthorhombic  $Ccca$   $\text{PtSn}_4$  lattice and  $a'$ ,  $b'$ ,  $c'$  indicate the Brillouin zone. Note that  $a'$  and  $b'$  are not of same length. Frequencies associated with ten sheets of Fermi surface (B1,  $\alpha$ ,  $\beta_1$ ,  $\beta_2$ ,  $\gamma$ ,  $\delta$ ,  $\eta_1$ ,  $\eta_2$ ,  $\epsilon$  and B4), marked in the plot, were calculated (see Table 1).

### Acknowledgement

This work was supported by the ERC advanced researcher grant no. 227378 and the FWF (Austrian Science Fund, project P19458-N16).

### References

- [1] B. Kunnen, D. Niepmann, W. Jeitschko, *Journal of Alloys and Compounds* 309 (2000) 1-9.
- [2] E. Mun, H. Ko, G. J. Miller, G. D. Samolyuk, S. L. Budko, P. C. Canfield, *Phy. Rev. B* 85 (2012) 035135.
- [3] M. Rotter, H. Müller, E. Gratz, M. Doerr, M. Loewenhaupt, *Rev. Sci. Instrum.* 69 (1998) 2742.

## **Solid Compounds of Transition Elements II**

10.4028/www.scientific.net/SSP.194

## **Quantum Oscillations in Ultra Pure PtSn<sub>4</sub>**

10.4028/www.scientific.net/SSP.194.88